Forthcoming in Physics of The Earth and Planetary Interiors, DOI :10.1016/j.pepi.2007.05.001

Magma Flow Instabilities in a Volcanic Conduit: Implications for Long-Period Seismicity

Alina J. Hale

Fax: +61 7 3346 4134

Email: alinah@esscc.uq.edu.au

Earth Systems Science Computational Centre (ESSCC), Australian Computational Earth Systems Simulator (ACcESS), The University of Queensland, QLD 4072, Australia

Silicic volcanic eruptions are typically accompanied by repetitive Long-Period (LP) seismicity that originates from a small region of the upper conduit. These signals have the capability to advance eruption prediction, since they commonly precede a change in the eruption vigour. Shear bands forming along the conduit wall, where the shear stresses are highest, have been linked to providing the seismic trigger. However, existing computational models are unable to generate shear bands at the depths where the LP signals originate using simple magma strength models. Presented here is a model in which the magma strength is determined from a constitutive relationship dependent upon crystallinity and pressure. This results in a depth-dependent magma strength, analogous to planetary lithospheres. Hence, in shallow highly-crystalline regions a macroscopically discontinuous brittle type of deformation will prevail, whilst in deeper crystal-poor regions there will be a macroscopically continuous plastic deformation mechanism. This will result in a depth where the brittle-ductile transition occurs, and here shear bands disconnected from the free-surface may develop. We utilize the Finite Element Method and use axi-symmetric coordinates to model magma flow as a viscoplastic material, simulating quasi-static shear bands along the walls of a volcanic conduit. Model results constrained to the Soufrière Hills Volcano, Montserrat, show the generation of two types of shear bands: *upper-conduit shear bands* that form between the free-surface to a few 100 metres below it and *discrete shear bands* that form at the depths where LP seismicity is measured to occur corresponding to the brittle-ductile transition and the plastic shear region. It is beyond the limitation of the model to simulate a seismic event, although the modelled viscosity within the discrete shear bands suggests a failure and healing cycle time that supports the observed LP seismicity repeat times. However, due to the paucity of data and large parameter space available these results can only be considered to be qualitative rather than quantitative at this stage.

Keywords: Volcanology, Magma flow, LP seismicity, Eruptions, Shear bands

1. Introduction

At depths of around 100 kilometers the mantle is at high enough temperatures and pressures to melt, forming magma, which rises towards the Earth's surface due to buoyancy. The magma sometimes pools in large chambers at depths of several kilometers to ten's of kilometers. From the chamber to the free-surface the ascent of magma is not simple to model because of its complex rheology. Magma is comprised of silicate liquid, crystals and gas bubbles which vary in quantity during ascent and flow. Very small changes in the quantity of these components, changes in state variables values such as pressure and temperture, as well as changes in conduit shape/size can result in enormous changes in the eruption behaviour (Melnik and Sparks, 1999). Volcanoes that form from partial melting in subduction zones generally produce the most viscous magma and contain large amounts of dissolved volatiles. Such volcanic eruptions can form a *lava dome* when the extruded lava is so viscous it can't flow freely away from the vent. Collapse events are a common and important part of the evolution of lava domes, but can have devastating consequences, resulting in block and ash avalanche deposits, pyroclastic flows, surges and the generation of tsunamis if they enter the sea (Voight, 2000). In addition to this, once the pressure has been released during a collapse event the remaining volatile-rich lava may erupt explosively.

Accompanying silicic volcanic eruptions are commonly three seismic signals; *Volcano-Tectonic* (VT) events thought to be indicative of rock fracture, *Long-Period* (LP) events characterized by their harmonic signature and interpreted as oscillations in a fluid-filled resonator (Kumangai and Chouet, 1999), and *Hybrids* a mixture of LP and VT events (Neuberg et al., 2000). Changes in eruption vigour and lava dome collapse events are commonly preceded by swarms of hybrid and LP earthquakes providing the opportunity for exploring eruption prediction (Miller et al., 1998; Calder et al., 2002). However, an understanding of the origin of LP events has yet to be achieved, and since their occurrence does not always guarantee a volcanic response, they are not a reliable forecasting tool. Shear bands, localised regions of high strain that form along the conduit wall where the shear stresses are highest, have been linked to providing the seismic trigger for LP events. However, using simplified magma strength models shear bands are unlikely to develop at the depths where these signal occur (Neuberg et al., 2005; Hale and Mühlhaus 2007). In addition to this, simplified magma strength models produce a continuous shear band along the entire length of the upper conduit, suggesting that any extruded lava should form along shear boundaries when LP events occur, which is not the case (Miller et al., 1998; Watts et al., 2002).

Silicic magma is non-Newtonian below its liquidus temperature (Pinkerton and Stevenson, 1982). For this reason we simulate magma flow using a viscoplastic model based upon the well-documented strain-softening behaviour of magma (Webb and Dingwell, 1990, Voight et al., 1999; Hale and Wadge, 2003). Our model determines magma strength from the crystallinity and pressure, resulting in a depth-dependent magma strength. Using the Finite Element Method (FEM) we model quasi-static shear bands forming at the brittle-ductile transition, at depths where LP seismicity occurs, corresponding to the plastic shear region. However, it is beyond the limitation of the model to simulate a seismic event. Our model can generate shear bands at LP seismicity depths without the need for a continuous shear band along the upper conduit wall. The generation of shear bands are also found to have a large effect upon the over-pressure, predominantly in the upper conduit. This may provide an additional mechanism for pressure increase and decrease in the upper-conduit that may be responsible for the observed volcano flank tilt, essentially the inflation and deflation of the volcano flanks. Pressure changes as large as several MPa's are modelled to develop at depths of 100s m, values suitable to generate the observed tilt.

In the following section we discuss the observational evidence associated with LP events and how this information can be used to constrain our model. Following this, in Section 3, we discuss the equations used in our model and the computational techniques used. A yield strength envelope is used to determine the magma strength at depth and this is discussed in Section 4. Section 5 provides model results with a discussion and conclusions presented in Sections 6 and 7 respectively.

2. Observational Evidence

LP seismic signals are commonly observed at the Soufrière Hills Volcano (SHV), Montserrat, where the trigger location is calculated to be at depths of approximately 1000 – 1400 metres below the conduit exit (e.g. Green and Neuberg, 2005; Neuberg et al., 2005; Rowe et al., 2004) (Fig. 1). LP events are small in magnitude and repeat times between successive events are typically minutes to hours ($10^{2.5}$ to $10^{4.5}$ seconds). During seismic swarms LP earthquakes can be highly repetitive with the time between consecutive events found to be less than 2% (Green and Neuberg, 2005). The similarity of the waveforms points to a repeatable non-destructive source mechanism that is highly periodic and can repeat for hours on end. It is also observed that the source locations can remain stable for at least 6 days during periods of vigorous magma extrusion and that the response time between similar events can be as short as 8 seconds, requiring a source mechanism which is easily recharged (Green and Neuberg, 2005).

Lava dome growth at the Soufrière Hills Volcano has frequently been accompanied by repetitive cycles of earthquakes, ground deformation, degassing and explosions (Voight et al., 1999). The cyclic behaviour can occur on a wide range of timescale but here we are concerned with cycles of activity that repeat with periods of hours to days. That is, cycles that are not accompanied by Vulcanian explosions that occur on timescales of weeks to months. Deformation of the volcano flanks have been measured using tilt-metres but it has also been observed that large fractures and seismically triggered landslides periodically occur indicating that the volcano flanks occasionally come under severe stress (Voight et al., 1999). The origin of the tilt signal occurs in the shallow (less than 1000m) top of the conduit and the mechanism for the tilt is thought to be pressurization from gas exsolution. Pressure build-up in the conduit inflates the edifice of the volcano and upon the movement of magma and release of gas the edifice deflates (Voight et al., 1999). The cycles are therefore thought to reflect unsteady conduit flow of volatile-rich magma experiencing gas exsolution.

The pressure build-up in the conduit may also be responsible for triggering shallow seismicity. LP signals are observed to coincide with the point at which flank inflation starts to decelerate (the point of inflexion), suggesting that the same process that initiates seismicity could also be initiating the depressurisation process (Green and Neuberg, 2005). The amount of tilt from edifice inflation can be used as a pressure gauge. Although half-space elastic, or Mogi, models of the flank inflation and deflation cycles observed in May 1997 suggest unrealistically large pressure changes of 60 MPa within 1000 m of the surface (Voight et al., 1999). The tensile strength of the edifice at shallow depths is estimated to be less than 10MPa (Sparks, 1997). While, isotropic pressure models using a pressure source low enough to prevent edifice failure indicate that a fluid-saturated body greater than 200 metres is required, although the conduit radius is only 15 metres (Widiwjayanti et al., 2005). Green et al., (2006) propose an alternative mechanism, suggesting that surface deformations recorded at tilt-metres could be from shear stresses within the upper conduit rather than from a large pressure source. Considering vertical traction along the conduit walls, the location for the build-up of shear stresses required to generate the observed tilt is calculated to be approximately 160 to 360m below the conduit exit, with traction values between 0.5 and 1.5MPa. These high shear stresses within the conduit suggest the development of shear bands (Green and Neuberg, 2006).

Observational evidence links earthquake swarms, due to rockfall activity from the dome surface, with cyclic lava dome emplacement. Rockfalls, as measured by the seismic network, correlate well with the extrusion rate for medium to high rates, less so for low rates (Calder et al., 2005). Typically, during cyclic deformation periods, lava dome growth will stagnate and the accompanying rockfall activity from the dome is also reduced. Although the free-surface extrusion rate drops, the deep driving pressure remains high resulting in shallow pressurisation (Miller et al, 1998). LP earthquakes mark a change in regime of the upper conduit (Neuberg et al., 2006). Pressure build-up in the shallow conduit eventually forces lava to extrude at the free-surface, causing some endogenous (intrusive) inflation and exogenous (extrusive) displacement at the dome's surface, commonly with steaming fissures (Sparks and Young, 2002). At the peak of tilt deformation and during dome deflation lava is commonly extruded via slip along ductile shear faults with grooved surfaces. The generation of a new lava flow pathway is marked by acceleration in extrusion rate and an increase in the amount of rockfall activity from the advancing lava (Watts et al., 2002). Changes in extrusion rate are commonly related to major switches in the direction of lava dome growth. Resulting in the development of shear lobes, that move from the vent along shear boundaries (Watts et al., 2002). Although enhanced extrusion rates from crystal rich flows suggest the development of shear boundaries during these cyclic events (Green and Neuberg, 2006), observations by Watts et al. (2002) show that the whole range of structures extruded on Soufriere Hills Volcano, from spines to low-viscosity flows, can form with hybrid earthquakes present. This suggests that shear boundaries observed at the conduit exit are not a necessity during hybrid earthquake activity.

2.2 Seismic Trigger Mechanism

Hybrid earthquakes are made up of an initial high-frequency onset followed by a long-period coda, the LP event. The triggering mechanism responsible for the high-frequency onset is highly debated and has been linked to numerous sources, from the slick-slip motions of magma plugs, flow instabilities in the conduit to periodic release of gas-ash mixtures into open cracks. For completeness, details of some of the proposed trigger mechanisms are given here, but the list is by no means exhaustive.

Aki et al. (1977) originally suggested that the trigger may be from fluid-filled cracks. Chouet (2003) advanced upon this model to suggest that its origin could be from the formation of a shock wave associated with the compound choking of gas flow through the crack. Another trigger mechanism model uses the widely regarded explanation for earthquakes as stick-slip instabilities along a fault boundary due to stress concentration. By considering the stick-slip behaviour of industrial polymers Denlinger and Hoblitt (1999) relate this property to the cyclic behaviour of magmas. They suggest that the oscillatory behaviour originates from Newtonian flow of compressible magma through a volcanic conduit, combined with a stick-slip instability along the conduit wall. Extrusion rate oscillations in a volcanic conduit have been modelled by Wylie et al. (1999) and Melnik and Sparks (1999) to occur due to a volatile and crystal-dependent magma viscosity. These models produce oscillatory patterns in extrusion rates for a critical range of input flow rates, which they relate to oscillating patterns of ground deformation, seismicity and non-linear flow, but they do not explicitly discuss the seismic trigger mechanism. Recently, Balmforth et al. (2005) modelled volcanic tremor occurring from magma flow instabilities in a conduit, analogous to roll waves, although they acknowledge that the physical conditions required for this form of instability are geologically inconsistent with silicic magma eruptions.

Recent observational evidence has supported the idea that the triggering mechanism for the high-frequency onset originates from a flow instability in the form of a shear boundary (Tuffen et al., 2003). Tuffen et al. (2003) argue that stress accumulation in viscous magma can lead to brittle shear within the magma column, resulting in the formation of shear fractures through which gas and ash can escape. Fine-grained fragments of magma within shear boundaries are interpreted as being generated by the shear fracture of magma in the glass-transition. Sedimentary structures formed by the fine grained material suggest transient pressure gradients from the flow of fluids through these cracks (Tuffen and Dingwell, 2005). Subsequent welding of the particulate material may allow for a repeated fracture, resulting in a cycle of stress accumulation to failure and subsequent healing, providing an explanation for the repetitive nature of the LP seismic trigger mechanism.

Following the high-frequency trigger a resonator is required to capture the seismic energy and to form the LP coda. There are two main models used to describe the resonator. Kumagai and Chouet (1999) suggest that the emission of ash-laden gas into an open crack acts as the resonator. This model requires a pressure transient in a resonating crack a few centimetres wide to generate the observed LP signals. Alternatively, Neuberg et al. (2006) suggest that the magma filled dyke or conduit, which is in close vicinity to the high-frequency trigger location, generates the LP coda. This is achieved by the resonance of the magma column, triggered by the movement of gas released from batches of gas-rich magma. The fracture energy produced from brittle failure of the magma is trapped within the conduit due to a high impedance contrast and requires a conduit section several 100 metres in length and a conduit diameter of several 10's metres.

2.3 Computational Model

Observational evidence supports the idea that long-period seismicity at silicic volcanoes may be measuring the repeated fracture energy generated from shear bands within a magma conduit (Neuberg et al. 2005). However, no numerical model has simulated shear bands to the depths at which LP seismicity occurs. Denlinger and Hoblitt (1999) model the depths at which stick-slip can occur to be approximately 500m from the free-surface for the frequency of tilt and seismicity observed at Soufrière Hills Volcano. While Neuberg et al. (2005) and Hale and Mühlhaus (2007) use Finite Element Method (FEM) techniques for shear band development, but can only model shear bands to depths of 830 and 700 metres respectively using values appropriate for Soufrière Hills Volcano. In addition, all these models consider a yield strength that produces a continuous shear band along the entire length of the upper conduit. This suggests that the lava extruded at the free-surface is always along shear boundaries when LP seismicity occurs, which is not the case (Miller et al., 1998; Watts et al., 2002). Hence, we are neglecting something fundamental; a change in the constitutive relation describing the magma properties at depth and we model this here.

Explicitly modelling LP seismicity is beyond the limitation of this model; our model ignores an elastic-brittle contribution to the rheology, and without this seismicity can not be directly modelled. However, shear bands are characterised by localised high shear stresses resulting in plastic yielding. Incorporating an elastic-brittle rheology would lead to the generation of brittle failure within the shear bands due to shear-stress accumulation. Our model calculates the location of plastic failure along the edges of the volcanic conduit, shears bands, and reconciles them to LP seismicity given their depth and phenomenology. We purposely don’t discuss which fluid is being invoked for LP resonance because this is not our modelling goal. A brittle-failure triggering mechanism may invoke an LP coda using either of the resonance mechanisms described in this paper.

3. Model Development

An axi-symmetrical conduit model has been developed that solves the mass continuity and momentum equations using the parallelized FEM based partial differential equation solver eScript and the FE library Finley (Gross et al., 2007). We describe the model domain, equations and computational techniques here.

3.1 Model Domain

A cartoon of the model domain is shown in Figure 1. The model is generic in nature, but the physical parameters of the Soufrière Hills Volcano are used to characterise and test the model behaviour. Modelled for simplicity is the conduit-only region, of uniform radius between the magma chamber and conduit exit. The length of the conduit is 5 km and has a 15 metre radius (Barclay et al., 1998). The axi-symmetric cylindrical conduit is discretised using 5000 x 15 uniform elements with quadratic shape functions (8 nodes per element) in conjunction with 4 point Gauss integration for the element matrices.

[Location of figure 1]

3.2 Momentum Equations

The flow of magma in the conduit is treated as a viscoplastic fluid using the axi-symmetric Stokes equations with no inertial effects (see Appendix A). We define the Reynolds number as $\mathrm{Re} = \rho_{lava} VL / \eta_{lava}$, where ρ_{lava}, V and L are the density of the lava, characteristic velocity and characteristic length scale respectively. Using V as the average velocity of a Hagen-Poiseuille flow in the conduit with a pressure gradient of

P^0/h for the constant pressure head boundary condition we obtain $V = a^2 h/(8\eta_{lava} P^0)$. Assuming L=h gives values for Re in the order of 10^{-11}, justifying our neglect of inertia. The constitutive equation for a Newtonian, viscous material is given by equation 1 using Einstein's summation convention for tensor notation. Viscoplasticity enters this model as a change in the viscosity as determined by the strain-rate and magma yield strength as discussed in Section 3.3.

$$\sigma'_{ij} = 2\eta D'_{ij}, \tag{1}$$

where $\sigma'_{ij} = \sigma_{ij} + P\delta_{ij}$ is the deviatoric stress, $P = -\frac{1}{3}\sigma_{kk}$ the pressure, η is the viscosity and $D'_{ij} = D_{ij} - \frac{1}{3}D_{kk}\delta_{ij}$ is the deviatoric stretching tensor. Pressure and velocity are solved using a modified Uzawa scheme as discussed in Appendix B (Zienkiewicz and Taylor, 2000). The boundary condition of no-slip is applied at the conduit walls.

3.3 Shear Bands

The magma rheology is based upon the well-documented strain-softening behaviour of magma (e.g. Webb and Dingwell, 1990; Pikerton and Stevenson, 1982). In a static state suspended particles or crystals become organised into an ordered structure held together by inter-particle forces (Balmforth and Craster, 2000). This structure is able to resist weak stress, in the form of a yield stress, before breaking apart and flowing. However, the microstructure is not likely to instantaneously disintegrate as the fluid flows. Instead, material structure will be progressively broken up by increasing shear stresses and the fluid will experience shear thinning above the yield point (Pinkerton and Stevenson, 1982). A viscoplastic constitutive relation is therefore used to replicate the microstructural response of magma flow with yield strength.

Shear bands form in materials as a result of severe shear and are commonly precursors to failure (Regenauer-Lieb and Yuen, 2003). Localized shear bands will form if the underlying flow or deformation experiences a particular type of instability. The instability expresses itself mathematically in a change in the type of the tangential boundary value problem. For strain-rate independent problems this change is usually from elliptic to hyperbolic behaviour, i.e. when the governing partial differential equations possess real characteristics. In pressure-sensitive materials the instability may arise because of a mismatch between the pressure sensitivity and the dilatancy factor and/or strain softening e.g. due to micro-cracking. Another important shear band generating mechanism is related to shear heating and thermal feedback due to a strongly temperature-dependent viscosity. Thus the latter mechanism is only particularly relevant for high Péclet number flows.

Our visco-plastic model generates shear bands by considering a yield strength (Rudnicki and Rice, 1975). The yield strength τ_Y provides the limit to the acceptable stress state in the material. We use an effective viscosity defined as $\eta_{eff} = \min[\eta, \eta_Y]$ in the solution of the velocity-pressure problem, where η is the empirical Newtonian viscosity (as discussed in Section 3.4) and the shear viscosity $\eta_Y = \tau_Y / \dot{\gamma}$. The definition of η_{eff} ensures that $\tau - \tau_Y \leq 0$ everywhere and $\tau - \tau_Y = 0$ if $\eta_{eff} = \eta_Y$. Since $\dot{\gamma}$ is unknown initially the solution has to be determined iteratively, and up to 10 iterations are required before convergence is obtained. During the iterations the plastic zone typically narrows until it is localized in a band approximately one element wide.

3.4 Rheology Equations

Magma contains crystals, melt and bubbles which vary in proportion during ascent and flow. The role of bubbles in the simulation is ignored because the focus of this study is on Soufrière Hills andesitic magma which contains crystals that more significantly affects the viscosity of the magma than bubbles (Pal, 2003; Costa, 2005). Soufrière Hills andesitic magma is rich in crystals in the reservoir where it is inferred to have a crystal content of approximately 60 to 65% (Sparks et al., 2000). At the start of the 1995-1998 eruption, the lava was extruded at low rates and had a highly crystalline groundmass with only 5-15% residual rhyolitic melt (Barclay et al., 1998). Samples from periods of more rapid dome growth have higher glass contents, up to 30%. During ascent, crystals form primarily due to the change in pressure rather than temperature. Crystal growth begins when the temperature of the magma or lava becomes lower than its liquidus temperature. Hence, exsolution of water from the melt can therefore induce crystallization by increasing the liquidus temperature (Cashman and Blundy, 2000). The equilibrium crystal volume fraction ϕ_{eq} in the melt phase is found from the liquidus temperature $T_{liq}(P)$ that changes during crystallization due to the progressive chemical change of the melt (Sparks, 1997),

$$\phi_{eq} = \frac{A(P)(T - T_{liq}(P))}{B(P) - T}. \qquad (2)$$

Here $A(P)$ and $B(P)$ are functions of the pressure and T is the temperature (Melnik and Sparks, 2005).

The viscosity of the magma is calculated using an empirical equation for the melt component η_m given as a function of the water content and temperature (Hess and Dingwell, 1996). The water content in the magma is given by Henry's solubility law $c = \alpha_S \sqrt{P}$, where α_S is the solubility coefficient and P is the pressure in Pascals. Petrological studies indicate that the magma chamber has dissolved water content in the melt phase of 4.3% (Barclay et al., 1998). The crystal volume fraction has a very large influence upon η the total viscosity (Melnik and Sparks, 2005), and is represented by equation 3 with the coefficients given in Table 1.

$$\eta = \vartheta(\phi)\eta_m, \tag{3}$$

$$\log\left(\theta(\phi) \big/ \theta_0 \right) = \left(\arctan\left(\xi\left(\phi - \phi_0 \right) \right) + \pi / 2 \right),$$

where $\phi = \phi_{eq}$ is the equilibrium crystal volume fraction.

3.5 Initialising the Model

The temperature of the magma in the conduit is assumed to be in equilibrium, and thus isothermal at 1123°K, a common and valid assumption since the thermal conductivity of magma is very low (Melnik and Sparks, 1999). We also assume that shear bands form instantaneously so that isothermal conditions prevail. The conduit walls are assumed to be at the same temperature as the magma. This is justified by assuming the eruption is long-lived, the case for Soufrière Hills Volcano, and therefore the conduit walls have been pre-heated.

Magma flow in a conduit is often unsteady with the extrusion rate varying by a large amount in time (Melnik and Sparks, 1999). This is a result of the complex feed-back processes primarily resulting from crystallisation kinetics, resulting in a temporal change in pressure and viscosity along the conduit length. However, we need an initial crystallinity, pressure and viscosity for our magma within the conduit from which to initialise our model. The simplest starting point is to assume that the flow is initially stationary. By making the assumption that the magma has remained stationary for a significant amount of time, it is appropriate to assume that the crystal content is in equilibrium with the pressure field (Eqn. 2). A stationary magma column also implicitly implies that no shear bands currently exist within the conduit at the start of the simulation.

From this initial magma state we need to initiate the flow of magma within the conduit. This is achieved by applying an over-pressure (total pressure minus magma-static pressure) from the magma chamber. Over time-scales associated with magma ascent in the conduit, the magma chamber key variables are assumed to be constant due to its large volume with respect to the lava dome and conduit. Volcanic eruptions require an over-pressure in the magma chamber to drive the magma to the free-surface, but the build up of this over-pressure is likely to be a very slow process (G. Wadge pers. comm.). Since our model is not transient at this stage, we need to make the assumption that an over-pressure change occurs that is rapid and large enough to drive the magma to high enough extrusion rates to generate shear bands. A source of significant over-pressure change can be achieved by removing a lava dome and or viscous cap existing at the conduit exit by means of a collapse event. A viscous cap may form due to the decompression of magma in the upper conduit or dome, which then enhances substantially the density and the resistance to flow (Diller et al., 2006). The removal of the dome and viscous cap transfers a driving pressure to the magma in the conduit enabling flow.

The initial pressure gradient from which to initialise the magma properties in the conduit (crystallinity, water content and Newtonian viscosity) thus comprises of a linear component from the magma-static pressure plus a constant over-pressure from the weight of the lava dome plus any additional force due to a viscous plug. Following the lava dome and viscous-cap removal, assumed to occur instantaneously, the conduit exit is maintained at atmospheric pressure. We do not claim that these are ideal initial conditions, but they are a necessary simplification with which to initialise our model. However, even with such a simplification our idealised model allows us to model the location of shear bands and we revisit this simplification and its implications in the discussion. Future modelling efforts will concentrate upon making our model transient so that it is possible to simulate the evolution of shear bands, temporal changes in the pressure within the conduit as well as changes in extrusion rate over time.

4. Yield Strength Envelope

The strength of brittle rocks increases with confining pressure, decreases with temperature, and deformation results from repeated shear fracturing (Albert et al., 2000).

In contrast, ductile deformation in rocks occurs due to plastic flow, which produces limited permanent strains at high stresses when the yield strength of the mineral grains is reached (Kearey and Vine, 1996). Which constitutive relationship controls the mode of deformation is governed by the material properties and external conditions (Regenauer-Lieb et al., 2006). This is analogous to planetary lithospheres where a common method for determining the depth-dependent strength combines Byerlee's (1978) rule for frictional slip of rocks with a yield stress for solid-state creep to determine a *yield strength envelope*. A yield strength envelope for magma can be calculated by determining what mechanism will make the magma mechanically weakest at any depth. It can be expected that as for the lithosphere, in shallow highly-crystalline regions a macroscopically discontinuous brittle type of deformation will prevail, whilst in deeper crystal-poor regions there will be a macroscopically continuous plastic deformation mechanism.

Deformation experiments on crystalline lava show that the mechanical behaviour is best described as a brittle solid (Sparks et al., 2000), suggesting a pressure-sensitive yield stress such as the Drucker-Prager yield criterion (Eqn. 4),

$$F = \tau - \tau_{Y\_DP} + \mu_f P \leq 0 . \qquad (4)$$

The yield stress at zero pressure is $\tau_{Y\_DP} = \dfrac{6c\cos\theta}{\sqrt{3}(3-\sin\theta)}$, with c the cohesion, $P = -1/3\sigma_{ii}$ is the pressure and $\mu_f = \dfrac{6\sin\theta}{\sqrt{3}(3-\sin\theta)}$ is the pressure sensitivity factor with θ the friction angle. For malleable magma the formation of a continuous crystal network will provide the yield strength (Saar et al., 2001). Three-dimensional models of crystal networks calculate the generation of a yield strength given by equation 5,

$$\tau_{Y\_S} = \tau_{Y\_0}\left[\frac{\phi/(1-\phi_c)}{(1-\phi)/\phi_m}\right]. \tag{5}$$

Here ϕ_c is a critical crystal volume fraction at which the network can first form, ϕ_m the maximum crystal volume fraction, beyond which the magma behaves as a brittle-solid, and τ_{Y_0} is the total interparticulate cohesion (Saar et al., 2001). Plagioclase, the predominant crystal for Soufrière Hills Volcano magma, modelled as randomly orientated prisms produce critical crystal volume fractions of between 0.08 and 0.2 (Saar et al., 2001). The maximum crystal volume fraction which determines the transition to a solid is uncertain with ϕ_m = 0.74 corresponding to the maximum packing fraction for uniform spheres. It is observed that for lava structures with shear surfaces, experiencing solid-like deformation, to be extruded at Soufrière Hills Volcano requires a crystal volume fraction in excess of approximately 0.7 (Watts et al., 2002). Unfortunately, little data exists to constrain the magnitude of the yield strength with values ranging from approximately 10^3 to 10^8 Pa (e.g. Blake, 1989; Lyman et al., 2005; Simmons et al., 2005; Pinkerton and Stevenson 1992). The yield strength envelope for magma can be described by combining the constitutive relationships, equations 4 and 5, as identified by equation 6.

$$\tau_Y = \frac{\tau_{Y\_DP}\tau_{Y\_S}}{\tau_{Y\_DP} + \tau_{Y\_S}}, \tag{6}$$

where $\tau_Y \approx \tau_{Y\_DP}$ when $\tau_{Y\_S} >> \tau_{Y\_DP}$, and $\tau_Y \approx \tau_{Y\_S}$ when $\tau_{Y\_S} << \tau_{Y\_DP}$.

Using the crystallinity calculated for Figure 1, a yield strength envelope can be identified as shown in Figure 2a. The relaxed Newtonian viscosity calculated from the pressure and crystal volume fraction in Figure 1 can be used to evaluate the maximum strain-rate experienced in the magma at the conduit wall before yielding occurs (Fig 2b). This simplified model suggests that there is a depth at which a minimum in the maximum strain-rate field occurs, directly below the brittle-ductile transition, which could be responsible for discrete shear bands. For example, a maximum crystal volume fraction of 0.8 and an extrusion rate of $1 m^3 s^{-1}$ (i.e. a strain-rate at the wall for a parabolic flow profile of approximately 3.8×10^{-4} s^{-1}) produces three points of intersection in Figure 2, at depths of 370, 1100 and 1500 metres. However our computational model that considers strain-localisation and monotonic convergence is required to confirm this.

[Location of figure 2]

5. Results

Table 1 gives values quoted in the literature for magma properties calculated or estimated to be appropriate for Soufrière Hills andesite. Parameter such as the temperature, density, initial crystallinity and pressure in the magma chamber are relatively well constrained from detailed petrological studies (e.g. Rutherford and Devine, 2003). However, magma strength parameters such as cohesion, friction angle and maximum crystal volume fraction are not well constrained. Some of this uncertainty is because the properties of semi-molten magma remains only limitedly studied. This is due to the considerable technical difficulties involved in deforming suitably large samples of lava at the high temperatures, pressures and strain rates that occur within lava domes (Ayling et al. 1995). As a result, we must rely on estimated strengths until further data is available, and it remains too computationally expensive to perform a full parameter sweep. Rather we use arbitrary values within the parameter range, meaning that the results should be considered to be conceptual rather than quantitative

[Location of figure 3]

Figure 3 shows results from one simulation with a maximum crystal volume fraction of 0.75, $\tau_{Y\_DP} = 10^4 Pa$ and $\mu_f = 0.087$ ($\theta = 4^\circ$). From left to right in Figure 3 we produce plots of velocity, strain-rate, shear stress and shear stress divided by the yield strength (effectively the plasticity). From these results we can extract the length and location of shear bands that form along the conduit wall, where the shear stress divided by the yield strength is exactly equal to unity. In Figure 3 this corresponds to a narrow band, one element wide, flush against the conduit wall within the red area of the plastic region. Figure 3 shows that there can be *upper-conduit* and *discrete* shear bands. Specifically, this simulation produces upper-conduit shear bands to a depth of 128m and a discrete shear band from 1037 to 1442m, a length of 405m. Upper-conduit and discrete shear bands are separated from each other due to the constitutive relationship used for the yield strength. As for the Earth’s lithosphere, the strength of the rocks is highest at the brittle-ductile transition (Regenauer-Lieb et al., 2006). The brittle-ductile transition in our model thus acts as a barrier, preventing upper-conduit and discrete shear bands interacting.

Models are solved for four maximum crystal volume fraction values appropriate for Soufrière Hills andesite (0.725 to 0.80) using $\tau_{Y\_DP} = 10^4 Pa$ and $\mu_f = 0.087$ ($\theta = 4^\circ$). The values chosen for τ_{Y_DP} and μ_f are appropriate for semi-molten magma (Simmonds et al, 2005). We use a range of magma chamber pressures to initiate flow up to a maximum over-pressure of 21.4 MPa. Figure 4 shows the extent of shear bands forming along the conduit wall for our simulations. Upper-conduit shear bands form to depths of 140 metres from the free-surface for driving pressures up to 137MPa. Depending upon the maximum crystal volume fraction, discrete shear bands occur at depths between 320 and 3000 metres. Results in Figure 4 show that by increasing the maximum crystal volume fraction, the region where discrete shear bands can form increases. However, the median depth of discrete shear bands is centred between approximately 950 metres (for ϕ_m = 0.80) and 1500 metres (for ϕ_m = 0.725) and is strongly dependent upon the maximum crystal volume fraction. The depth and length of discrete shear bands is very sensitive to the maximum crystal volume fraction. LP seismicity at Soufrière Hills Volcano originates at depths of approximately 1000 to 1400 metres below the conduit exit, consistent with the location of discrete shear bands in our model. As shown in Figure 2, it is the maximum crystal volume fraction that affects the location of the brittle-ductile transition, the cohesion and friction angle simply affect the magnitude of the yield strength. Thus, the maximum crystal volume fraction will determine the location of the brittle-ductile transition and where discrete shear bands will originate.

[Location of figure 4]

It is possible to model discrete shear bands in a conduit with no upper-conduit shear bands present when an appropriate cohesion and friction angle are used. In Figure 5 shear bands are modelled for $\tau_{Y\_DP} = 10^6 Pa$, $\mu_f = 0.71$ ($\theta = 42^\circ$) and ϕ_m = 0.775, again appropriate values for Soufrière Hills andesite according to Table 1, although these values are most appropriate for crystal-rich semi-solidified magma. Using these values produces discrete shear bands between 635 and 1680 m, centred about 1030 m up to a magma chamber pressure of 135MPa. Therefore, discrete shear bands can be generated without the need for upper-conduit shear bands. This result can explain the paradox as to why LP events are present during surface lava flow with and without shear boundaries. That is, upper-conduit shear bands are necessary for lava flow along shear boundaries originating at the conduit exit. However, it was observed that during the iterative process discrete shear bands would only form if the extrusion rate was high enough. The formation of upper-conduit shear bands has a significant effect upon the extrusion rate because the viscosity is largest in the upper part of the conduit. Thus, upper conduit shear bands may initiate discrete shear bands by modifying the extrusion rate.

[Location of figure 5]

Uncertainty in the parameters (Table 1) mean that the values used in Figures 4 and 5 are both valid for Soufrière Hills andesite. In reality it may be that the cohesion and friction angle dependent upon crystallinity and temperature, meaning that the yield strength in the upper conduit could change due to crystal growth and heat loss. Nakada et al. (1999) observe that over time the yield strength must increase in extruded lobes to allow their slope angle to increase. If this is the case, then the generation of upper conduit shear bands will be related to the extrusion rate due to crystallisation kinetics, with upper-conduit shear bands more likely to form at the lowest extrusion rates when crystallinity is highest.

Cyclic inflation and deflation of the volcano flanks as measured by tilt-meters is thought to be indicative of pressure changes within the upper conduit. Flank inflation results from the formation of an impeding viscous plug leading to the over-pressure from the magma chamber initially being transferred to shallow depths in the conduit (Diller et al., 2006). The removal of the plug results in the deflation of the volcano flanks due to a re-distribution of the pressure field. We use our model to evaluate the pressure field within the conduit. Figure 6 shows the pressure in the conduit with depth following the removal of the lava dome and viscous cap, for flow in the conduit without (i.e. Hagen-Poiseuille flow) and with shear bands. Naturally, the majority of the pressure change is in the upper conduit due to the highest viscosities experienced there.

[Location of figure 6]

Figure 6 doesn't really give a good indication of the change in pressure due to the influence of shear bands. A better indication is the pressure difference between flow in a conduit without shear bands (i.e. Hagen-Poiseuille flow) and flow with shear bands.

This does not produce a rigorous comparison, because the modelled flow without shear bands (Hagen-Poiseuille flow) has shear stresses that exceed the shear stress required for shear bands. However the viscosity field will be modified in the presence of shear bands, and this result show where the modification is largest. Figure 7 shows the change in pressure along the conduit due to the development of shear bands with (Fig 7a) and without (Fig 7b) upper-conduit shear bands. A positive pressure difference corresponds to a pressure drop, which relates to the deflation of the volcano flanks. Figure 7a shows that the largest change in over-pressure occurs in the upper conduit, and this is related to a pressure drop due to the formation of upper-conduit shear bands where the viscosity of the magma is highest. LP seismicity is commonly coeval with flank tilt, and is most intense during the peak of inflation, suggesting that shear boundaries necessary for plug removal are being developed. During this time LP seismicity is sometimes observed to occur simultaneously with ash and gas venting from cracks at the free-surface (Watts et al., 2002) probably due to an enhanced permeability. Thus shear stresses in the upper conduit may influence the tilt in addition to depressurisation (producing normal stresses) due to rapid degassing along cracks from fracture along the conduit wall.

[Location of figure 7]

Green et al. (2006) calculate that a stress change of 0.5 – 1.5MPa is enough to explain the amplitude of flank tilt observed for Soufrière Hills Volcano when the surface deformations are from shear stresses within the upper conduit. Close to the magma chamber maximum pressure (134.2 MPa) we model an upper-conduit pressure change of over 3.0MPa for magma flow with and without upper-conduit shear bands. However, since our models are intended to be conceptual we can only tentatively remark that the pressure magnitude and depth is approximately correct. Figure 7b shows that the pressure change in the conduit with no upper-conduit shear bands is minimal and deep, suggesting that flank-tilt is only significant when upper-conduit shear bands are present. This result is consistent with observational data which suggests that lava extrusion is predominantly along shear boundaries during flank tilt cyclicity episodes.

6. Discussion

Utilising a visco-plastic model with a depth-dependent yield strength results in discrete shear bands forming at the depths where LP seismicity occurs at Soufrière Hills Volcano, corresponding to the plastic shear region. Plastic shear has been proposed to explain deep earthquakes in subduction zones as a result of instabilities in flow (Hobbs and Ord, 1988). Also, the depth at which localized shear structures form is thought to be related to the brittle-ductile transition in the lithosphere (Regenauer-Lieb et al., 2006). Our model ignores an elastic-brittle rheology and without this seismicity can not be directly modelled. However, shear bands are characterised by localised high shear stresses resulting in plastic yielding. Incorporating an elastic-brittle rheology would lead to the generation of brittle failure within the shear bands due to shear-stress accumulation. The brittle-failure energy would then provide the trigger mechanism for LP seismicity.

We purposely don’t discuss which fluid is being invoked for the LP resonance. There is increasing evidence that much of the shallow seismicity used to monitor dome eruptions is triggered by the fracturing of lava (Tuffen and Dingwell 2005). It is possible that plastic failure within discrete shear bands could produce the seismic trigger at the depths where LP seismicity occurs. But it is beyond the limitation of our model and outside the context of the research presented to speculate how LP resonance occurs. However, brittle failure in shear bands will generate micro-cracking, porosity or damage growth resulting in a volume increase of between 1 and 10%. This could produce cracks which may support resonance in Kumagai and Chouet's (1999) model. Alternatively, a volume change could help initiate the LP code in Neuberg et al.'s (2006) model by aiding gas exsolution.

Following stress released by brittle failure the surrounding magma can experience relaxation resulting in the healing of the failure zone by welding. The viscosity within our discrete shear bands is modelled to be approximately $10^7 - 10^8$ Pa s, that suggests a failure and healing cycle time of the order of seconds (Tuffen et al., 2003). Unique LP waveforms identified during seismic swarms are observed to have a repeat time between events as short as 8 seconds which supports our modelled viscosity (Green and Neuberg, 2005).

A collapse event is not a realistic way to model magma flow in a conduit, but has been a necessary simplification for our model. Changes in the over-pressure field are prevalent at depths less than approximately 1000 metres below the conduit exit, but below this it is more stable (Sparks, 1997). This is apparent in Figure 6 which shows that even for a large change in pressure in the upper conduit, the pressure change at depth is very small. Hence the crystallinity and volatile content will not change significantly at the depths where discrete shear bands form. The timescales for microlite nucleation are on the order of days. During periods of sustained magma flow the crystallinity in the centre of the conduit may be lower due to crystallisation kinetics (Hale et al, 2007). However the largest strain-rates and hence shear stresses are likely to remain at the conduit walls due to a no-slip boundary condition. Magma viscosity is predominantly influenced by crystallinity and water content which are primarily dependent upon pressure and not temperature. Thus, at the conduit wall where magma flow is stationary, the crystal volume fraction and water content in the magma will be in equilibrium with the applied pressure. Hence the viscosity field is not expected to change much at depth at the conduit walls. Green and Neuberg (2005) show that LP seismic sources are extremely stable spatially and do not significantly evolve even through periods of high amplitude shallow deformation or dome collapse. Since only very small changes in magma properties are likely to occur at depth, this means that the location of discrete shears bands is not expected to change substantially in time.

It is possible that magma damage accumulation, through the generation of shear bands, could be transported to higher levels in the conduit if the magma is transported rapidly preventing healing through relaxation. There is commonly a large damage zone in the upper part of the conduit, possibly due to shear bands, and this damage is likely to be largest when the crystallinity is highest due to enhanced erosional capabilities. Hence, at depth in the conduit discrete shear bands may erode the surrounding conduit walls generating subsequent flow instabilities from geometrical effects and potentially fixing the location of the LP source.

7. Conclusions

Understanding long-period earthquakes has the capability to advance eruption prediction since they commonly precede a change in the eruption vigour. Shear bands forming along the conduit wall where the shear stresses are highest are thought to be capable of providing the seismic trigger. A model in which the magma strength is determined from a constitutive relationship, dependent upon crystallinity and pressure, results in a depth-dependent magma strength analogous to planetary lithospheres. This will result in a depth where the brittle-ductile transition occurs, and here shear bands may develop. We simulate shear localization and the generation of two types of shear bands: *upper shear bands* (forming between the free-surface to a few 100 metres below it) and *discrete shear bands* forming at the depths where LP seismicity occurs corresponding to the plastic shear region. However, due to the paucity of data and large parameter space our results can only be considered to be conceptual rather than quantitative at this stage. Plastic shear has been proposed to explain deep earthquakes in subduction zones as a result of instabilities in flow and this may also be the case for LP seismicity. The viscosity within these discrete shear bands suggests a failure and healing cycle time that supports the observed LP seismicity repeat times. In addition, our shear band model allows LP events to be present during the different lava extrusion styles, with and without upper-conduit shear boundaries. Our model provides a method for pressure to decrease in the upper-conduit, possibly responsible for flank tilt, due to the generation of shear bands. Pressure changes as large as several MPa's develop at depths of 100s m, values suitable to generate the observed tilt.

Acknowledgements

Thanks for insightful comments from M. A. O'Brien, D. Weatherley, D. Green, M. Brenna and H.-B. Mühlhaus. I thank two anonymous reviewers for help in significantly improving the manuscript. Support is gratefully acknowledged by the Australian Computational Earth Systems Simulator Major National Research Facility (ACcESS MNRF), The University of Queensland, and a UQ New Staff research grant.

Appendix A: *Escript* Formulation

The modelling library *escript* has been developed as a module extension of the scripting language Python to facilitate the rapid development of 3-D parallel simulations on the Altix 3700 (Gross et al, 2007). The finite element kernel library, *Finley*, has been specifically designed for solving large-scale problems on ccNUMA architectures and has been incorporated as a differential equation solver into *escript*. In the *escript* programming module Python scripts orchestrate numerical algorithms which are implicitly parallelised in *escript* module calls, without low-level explicit threading implementation by the *escript* user.

The *escript* Python module provides an environment to solve initial boundary value problems (BVPs) problems through its core finite element library *Finley.* A steady, linear second order BVP for an unknown function u is processed by *Finley* in the following template system of PDEs (expressed in tensor notation):

$$-(A_{ijkl}v_{k,l})_{,j} - (B_{ijk}v_k)_{,j} + C_{ikl}v_{k,l} + D_{ik}v_k = -X_{ij,j} + Y_i, \qquad \text{(A1)}$$

where the Einstein summation convention is used. *Finley* accepts a system of natural boundary conditions given by:

$$n_j(A_{ijkl}v_{k,l} + B_{ijk}v_k) + d_{ik}v_k = n_j X_{ij} + y_i \quad \text{on} \quad \Gamma_i^N \qquad \text{(A2)}$$

where n denotes the outer normal field of the domain and A, B and X are as for (A1). d and y are coefficients defined on the boundary. The Dirichlet boundary condition is also accepted:

$$u_i = r_i \text{ on } \Gamma_i^D \tag{A3}$$

where r_i is a function defined on the boundary. *Finley* computes a discretisation of (A1) from the variational formulation. The variational problem is discretised using isoparametric finite elements on unstructured meshes. Available elements shapes are line, triangle, quadrilateral, tetrahedron and hexahedron of orders one and two.

With both the *escript* and *Finley* technologies, complex models and very large simulations can be rapidly scripted and run easily. The code is fully portable, but optimized at this stage for the local SGI ALTIX super cluster.

Appendix B: Governing Equations

The constitutive equation for a Newtonian, viscous material reads:

$$\sigma'_{ij} = 2\eta D'_{ij}, \tag{A4}$$

where σ'_{ij} is the deviatoric stress, η the viscosity, D'_{ij} the deviatoric stretching. The stress-equilibrium equations in axi-symmetrical coordinates reads

$$\begin{aligned} &(r\sigma_{rr})_{,r} + r\sigma_{rz,z} - \sigma_{\theta\theta} + rf_r = 0 \\ &r\sigma_{zz,z} + (r\sigma_{rz})_{,r} + rf_z = 0, \end{aligned} \tag{A5}$$

where f is a body force. The Uzawa scheme (Arrow et al., 1958) is used to solve momentum equations (A5) with the condition of incompressibility, $v_{i,i} = 0$. The scheme is iterative and based on the idea to that for a given pressure P^- the momentum equation can be used to calculate a velocity v^+ The divergence of the new velocity field v^+ is used to calculate an increment ΔP for the pressure, see (Cahouet and Chabard, 1988).

$$\frac{1}{\eta}\Delta P = v_{i,i}^{=}, \tag{A6}$$

and then update the pressure P^+ with:

$$P^+ = P^- + \Delta P. \tag{A7}$$

The new pressure P^+ can now be fed back into the momentum equation to get a new improved velocity approximation. The iteration is completed if the relative size of the pressure increment in the L^2-norm is smaller than a given positive tolerance:

$$\|\Delta P\|_2 \leq Tolerance \quad \|P^+\|_2 \; with \, \|P\|_2^2 = \int P^2 dx\,. \tag{A8}$$

This criterion can be problematic in practice because slow convergence triggers termination but for the purpose of the paper this criterion is sufficient. Gross et al. (2007) discuss the solution of the momentum equation using the Uzawa scheme in more detail.

References

Aki, K., Fehler, M. and Das. S., 1977. Source Mechanism of volcanic tremor: fluid driven crack models and their application to the 1963 Kilauea eruption. J. Volcanol. Geotherm. Res., 86, 7095 – 7110.

Albert, R. A., Phillips, R. J. Dombard, A. J., and Brown, D. C., 2000. A test of the validity of yield strength envelopes with an elastoviscoplastic finite element model. Geophys. J. Int. 140, 399-409.

Arrow, K., Hurwicz. L., and Uzawa, H., 1958. Studies in Nonlinear Programming, Stanford University Press, Stanford.

Balmforth, N. J., and Craster, R. V., 2000. Dynamics of cooling domes of viscoplastic fluid. J. Fluid Mechanics, 422, 225-248

Balmforth, N. J, Craster, R. V and Rust, A. C., 2005. Instability in flow though elastic conduits and volcano tremor. J. Fluid Mech. 527, 353 – 377.

Barclay, J. Rutherford M. J., Carroll M. R., et al., 1998. Experimental phase equilibria constraints on pre-eruptive storage conditions of the Soufriere Hills magma. Geophys. Res. Letts. 25, 3437-3440.

Blake, S., 1989. Viscoplastic models of lava domes. In Lava flows and domes. (ed. Fink J. H.) 88-127 (Springer. Berlin).

Byerlee, J., 1978. Friction of rocks. Pure Applied. Geophys. 116, 615 - 626.

Cahouet, J., and Chabard, J. P., 1998. Some fast 3D finite element solvers for the generalized Stokes problems. Int. J. Num. Meth. Fluids. 8, 869 – 895.

Calder. E.S., Cortes. J.A., Palma. J.L., et al., 2005. Probabilistic analysis of rockfall frequencies during an andesite lava dome eruption: The Soufriere Hills Volcano, Montserrat. Geophys. Res. Letts. 32, L16309

Chouet, B. A., 2003. Volcano seismology. Pure Appl. Geophys. 160, 739 – 788.

Costa A., 2005. Viscosity of high crystal content melts: Dependence on solid fraction. Geophys. Res. Letts. 32, L22308

Denlinger, R. P. and Hoblitt, R. P., 1999. Cyclic behavior of silicic volcanoes. Geology 27, 459 – 462.

Diller, K., Clarke, A. B., Voight, B., and Neri, A., 2006. Mechanisms of conduit plug formation: Implications for Vulcanian explosions. Geophys. Res. Letts. 33, Art. No. L20302.

Green, D. N., Neuberg, J. and Cayol, V., 2006. Shear stress along the conduit wall as a plausible source of tilt at Soufriere Hills volcano, Montserrat, Geophys. Res. Letts. 33, Art. No. L10306.

Green, D. N. and Neuberg, J., 2005. Waveform classification of volcanic low-frequency earthquake swarms and its implication at Soufrière Hills Volcano, Montserrat. J. Volcanol. Geotherm. Res. 153, 51 – 63.

Gross, L., Bourgouin, L., Hale, A. J. and Muhlhaus, H.-B., Interface Modeling in Incompressible Media using Level Sets in Escript, Physics of The Earth and Planetary Interiors, In Press.

Hale, A.J., and Wadge, G., 2003. Numerical modelling of the growth dynamics of a simple silicic lava dome. Geophys. Res. Letts. 30, Art. No. 2003 OCT 10 2003

Hale, A. J. and Mühlhaus, H.-B., 2007. Modelling Shear Bands in a Volcanic Conduit: Implications for Over-Pressures and Extrusion-Rates. Earth. Planet. Sci. Letts., submitted.

Hess, K. U. and Dingwell, D. B., 1996. Viscosities of hydrous leucogranitic melts: A non-Arrhenian model. Am. Mineral. 81, 1297-1300.

Hobbs, B. E. and Ord, A., 1988. Plastic instabilities: Implications for the origin of intermediate and deep focus earthquakes. J. Geophys. Res. 93, 10521 – 10540.

Jousset P., Neuberg, J, and Jolly, A., 2004, Modelling low-frequency volcanic earthquakes in a viscoelastic medium with topography. Geophys. J. Int. 159, 776 – 802.

Kearey, P. and Vine, F. J., 1996. Global Tectonics, Second edition, Blackwell Science.

Kumangai, H. and Chouet, B. A., 1999. The complex frequencies of long-period seismic events as probes of fluid composition beneath volcanoes. Geophys. J. Int. 138, F7 – F12.

Lyman, A. W., Kerr, R. C., and Griffiths, R. W., 2005. Effects of internal rheology and surface cooling on the emplacement of lava flows J. Geophys. Res. 110, Art. No. B08207.

Melnik, O. E. and R. S. J. Sparks, 1999. Non-linear dynamics of lava dome extrusion. Nature 402, 37-41.

Melnik, O. E. and Sparks R. S. J., 2005, Controls on conduit magma flow dynamics during lava dome building eruptions. J. Geophys. Res. 110, doi:10.1029/2004JB003183.

Miller, A. D. ., Stewart, R. C., White, R. A, et al., 1998. Seismicity associated with dome growth and collapse at the Soufriere Hills Volcano, Montserrat. Geophys. Res. Letts. 25 3401-3404

Nakada, S., Shimizu, H., and Ohta, K., 1999. Overview of the 1990 – 1995 eruption at Unzen Volcano. J. Volcanol. Geotherm Res. 89, 1-22.

Neuberg, J. Luckett, R. Baptie, B. and Olsen, K., 2000. Models of tremor and low-frequency earthquake swarms on Montserrat. J. Volcanol. Geotherm Res. 101, 83-14.

Neuberg, J. W. Tuffen H, Collier L, et al., 2005. The triggering mechanism of low-frequency earthquakes on Montserrat. J. Volcanol. Geotherm. Res., 153, 37-50.

Pal, R., 2003. Rheological behavior of bubble-bearing magmas. Earth Planet. Sci. Letts. 207, 165-179.

Pinkerton, H. and Stevenson, R. J., 1992. Methods of determining the rheological properties of magmas at sub-liquidus temperatures, J. Volcanol. Geotherm. Res. 53, 47-66.

Regenauer-Lieb, K. and Yuen, D. A., 2003. Modeling shear zones in geological and planetary sciences: solid- and fluid-thermal-mechanical approaches. Earth-Science Reviews. 63, 295 – 349.

Regenauer-Lieb, K., Weinberg, R. F. and Rosenbaum, G., 2006. The effect of energy feedbacks on continental strength. Nature 442, 67-70.

Rowe, C. A., Thurber, C. H. and White, R. A., 2004. Dome growth behavior at Soufriere Hills Volcano, Montserrat, revealed by relocation of volcanic event swarms, 1995 – 1996. J. Volcanol. Geotherm. Res., 134, 199 – 221.

Rudnicki, J. W. and Rice, J. R., 1975. Conditions for localization of deformation in pressure-sensitive dilatant materials. J. Mech. Phys. Solids 23, 371-394.

Rutherford, M. J. and Devine, J. D., 2003. Magmatic conditions and magma ascent as indicated by hornblende phase equilibria and reactions in the 1995-2002 Soufriere Hills magma, J. Petrol. 44, 1433-1454.

Saar, M. O, Manga, M., Katharine, V. C. and Fremouw, S., 2001. Numerical models of the onset of yield strength in crystal-melt suspensions. Earth Planet. Sci. Letts., 187, 367 – 379.

Simmons, J., Elsworth, D., and Voight, B., 2005. Classification and idealized limi-equilibrium analyses of dome collapses at Soufrière Hills Volcano, Montserrat, during growth of the first lava dome: November 1995 – March 1998. J. Volcanol. Geotherm. Res. 139, 241-258.

Sparks, R. S. J., and Young, S. R., 2002. The eruption of Soufrière Hills Volcano, Montserrat (1995 - 1998): Overview of scientific results. Geological Society London Memoirs 21, 71 - 92.

Sparks, R. S. J., Murphy M. D., Lejeune A. M. , et al., 2000. Control on the emplacement of the andesite lava dome of the Soufriere Hills volcano, Montserrat by degassing-induced crystallization. Terra Nova, 12, 14 – 20.

Sparks, R.S.J., 1997. Causes and consequences of pressurisation in lava dome eruptions, Earth Planet. Sci. Lett. 150, 177 - 189.

Tuffen, H., Dingwell D. B., and Pinkerton H., 2003. Repeated fracture and healing of silicic magma generate flow banding and earthquakes? Geology 31 1089 – 1092.

Tuffen, H. and Dingwell, D., 2005. Fault textures in volcanic conduits: evidence for seismic trigger mechanisms during silicic eruptions. Bull. Volcanol. 67, 370-387.

Voight, B., Sparks R. S. J., Miller A. D., et al., 1999. Magma flow instability and cyclic activity at Soufriere Hills Volcano, Montserrat, British West Indies. Science 283, 1138-1142.

Watts, R. B., Herd, R. A., Sparks, R. S. J., and Young, S. R., 2002. Growth patterns and emplacement of the andesite lava dome at Soufrière Hills Volcano, Montserrat, Geological Society London Memoirs 21, 115 - 152.

Webb, S. L. and Dingwell, D. B., 1990. Non-Newtonian rheology of igneous melts at high stresses and strain-rates: Experimental results for Rhyolite, Andesite, Basalt and Nephelinite. J. Geophys. Res. 95, 15695 – 15701.

Wylie, J. J., Voight, B. and Whitehead, J. A., 1999. Instability of magma flow from volatile-dependent viscosity. Science. 285, 1883-1885.

Widiwijayanti, C., Clarke, A., Elsworth, D., et al., 2005. Geodetic constraints on the shallow magma system at Soufriere Hills Volcano, Montserrat. Geophs. Res. Letts. 32 L11309

Zienkiewicz, O.C. and Taylor, R.L., 2000. The Finite Element Method, Volume 3: Fluid Mechanics, 5th ed., Butterworth-Heinemann.

Figure legends:

Figure 1: Schematic of a volcano, showing a conduit connecting the magma chamber to the free-surface, with lava dome/flow at the conduit exit (not to scale). In reality the conduit may narrow at depth but it is assumed to be a constant radius for simplicity in this model. Also shown on the figure is the approximate depth at which LP seismicity and pressurisation responsible for volcano flank tilt occurs. Shown next to the schematic is how the crystal volume fraction (grey line) varies with depth when in equilibrium with a linear pressure field (black line) over the depth in the conduit.

Figure 2: Yield strength envelope (a) and strain-rate envelope (b) against depth in the conduit, zero corresponds to the free-surface. Figure a) shows four yield strength curves with depth for maximum crystal volume fractions of 0.725, 0.75, 0.75 and 0.8 as shown in the legend. The critical crystal volume fraction used is 0.1, $\tau_{Y\_DP} = 10^4 Pa$ and $\mu_f = 0.087$ ($\theta = 4^\circ$).Note the similarity to the yield strength envelope used for the Earth's lithosphere, i.e. Regenauer-Lieb et al. (2006). Figure b) shows the strain-rate when considering the relaxed Newtonian viscosity, as calculated from the crystal volume fraction, for maximum crystal volume fractions of 0.725, 0.75, .775 and 0.8 as shown by the legend.

Figure 3: Results from one simulation with a maximum crystal volume fraction of 0.75, $\tau_{Y\_DP} = 10^4 Pa$ and $\mu_f = 0.087$ ($\theta = 4^\circ$). From left to right are plots of velocity, strain-rate, shear stress and shear stress divided by the yield strength (effectively the plasticity) within the conduit. Shown is only half of the conduit, from the centre of the conduit at r=0 (left side of image) to the conduit wall at r=15m (right side of image). The conduit

radius has been stretched in the figures by a factor of 30 to better visualise the results along the entire 5km length of the conduit. Where the shear stress divided by the yield strength is exactly equal to unity shear bands develop. This corresponds to a shear band one element wide, flush against the conduit wall, within the red zone of the plasticity figure. Upper-conduit shear bands form to a depth of 128m and a discrete shear band forms from 1037 to 1442m, a length of 405m in this simulation.

Figure 4: Location of modelled shear bands in a conduit for $\tau_{Y\_DP} = 10^4 Pa$, $\tau_{Y\_s} = 10^3 Pa$ and $\phi_C = 0.1$. Black filled symbols correspond to the depth that upper-conduit shear bands form to (*Upper* in legend). Below this depth the development of discrete shear bands can develop. Grey filled symbols correspond to the depth at which discrete shear bands begin (*Discrete top* in legend) within the conduit and open symbols correspond to the depth these shear bands penetrate to (*Discrete bottom* in legend). The different symbols correspond to the maximum crystal volume fraction used. Circles correspond to 0.8, triangles for 0.775, squares for 0.75 and diamond for 0.75 as also shown in the legend. The shaded regions correspond to the areas where discrete shear bands can form for the different maximum crystal volume fractions modelled.

Figure 5: Location of modelled shear bands in a conduit for $\tau_{Y\_DP} = 10^6 Pa$, $\tau_{Y\_s} = 10^3 Pa$, $\phi_C = 0.1$ and $\phi_M = 0.775$ which only shows the development of discrete shear bands. Black filled symbols correspond to the depth that upper-conduit shear bands form to (*Upper* in legend). Grey filled symbols correspond to the depth at which

discrete shear bands begin (*Discrete top* in legend) within the conduit and open symbols correspond to the depth these shear bands penetrate to (*Discrete bottom* in legend).

Figure 6: Pressure field within the conduit, for flow in the conduit without (i.e. Hagen-Poiseuille flow) and with shear bands. The magma chamber pressure in this simulation was 143.2 MPa and used a maximum crystal volume fraction of 0.775, $\tau_{Y\_DP} = 10^4 Pa$ and $\mu_f = 0.087$ ($\theta = 4^\circ$).

Figure 7: Change in over-pressure with depth (zero corresponds to the free-surface) due to the formation of shear bands. The pressure change is calculated from the pressure modelled in the conduit for magma flow with no shear bands minus the pressure within the conduit following the instantaneous formation of shear bands. Thus a positive pressure corresponds to a pressure decrease resulting in the deflation of the volcano flanks. The legend in the figures corresponds to the magma chamber pressure. Both figures have a maximum crystal volume fraction of 0.775, $\phi_C = 0.1$, $\tau_{Y\_s} = 10^3 Pa$ and figure a) uses $\mu_f = 0.087$ and $\tau_{Y\_DP} = 10^4 Pa$ (i.e. upper conduit shear bands) whilst figure b) uses $\mu_f = 0.71$ and $\tau_{Y\_DP} = 10^6 Pa$ (i.e. no upper conduit shear bands). The change in over-pressure in the upper conduit is substantial when upper-conduit shear bands exist. However for no upper shear bands (b) the change in over-pressure is minimal.

Table 1: Parameters used in the model which are appropriate for magma extruded from Soufrière Hills Volcano.

Symbol	Parameter	Reference	Value
T	Initial Temperature	Rutherford and Devine (2003)	1123°K
ϕ_i	Crystal volume fraction in chamber	Sparks et al (2000)	0.6
ρ	Density	Melnik and Sparks (1999)	2350 kg.m^{-3}
P_0	Maximum over-pressure	Sparks (1997)	20 MPa
P_C	Maximum chamber pressure	Calculated	137.5 MPa
ξ	Parameter in effective viscosity function	Melnik and Sparks (2005)	8.6
θ_0	Parameter in effective viscosity function	Melnik and Sparks (2005)	1.4
ϕ_0	Parameter in effective viscosity function	Melnik and Sparks (2005)	0.69
c	Cohesion or yield stress at zero pressure	Blake, (1989); Lyman et al., (2005); Simmons et al., (2005); Pinkerton and Stevenson (1992)	10^4 - 10^8 Pa.
θ	Friction angle	Simmons et al., (2005)	0 – 45°
τ_{Y_0}	Total interparticulate cohesion	Blake, (1989); Lyman	10^4 – 10^8 Pa

		et al., (2005); Simmons et al., (2005); Pinkerton and Stevenson (1992)	
ϕ_C	Critical crystal volume fraction	Saar et al., (2001)	0.08 – 0.20
ϕ_M	Maximum crystal volume fraction	Saar et al., (2001); Watts et al., (2002)	0.74 – 0.80

Figure1:

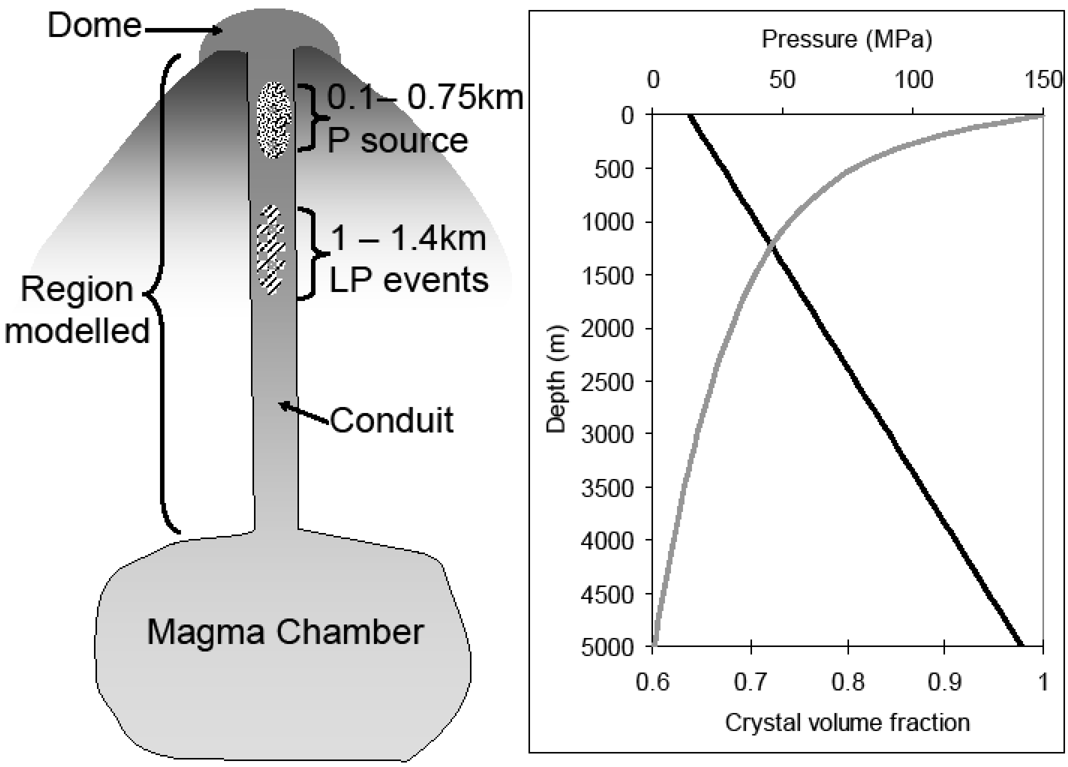

Figure2a:

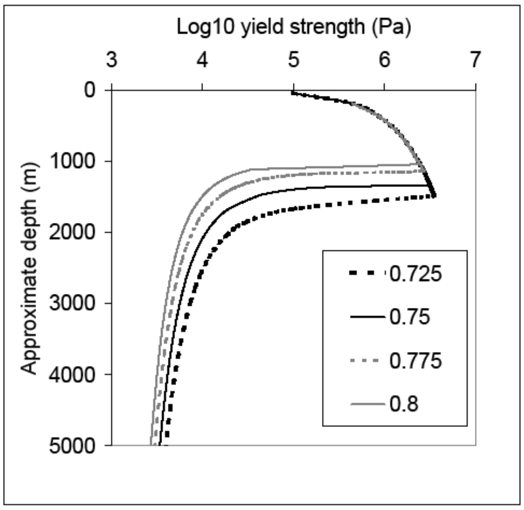
Log10 yield strength (Pa)
3
4
5
6
7
0
1000
2000
3000
4000
5000
Approximate depth (m)
0.725
0.75
0.775
0.8

Figure 2b:

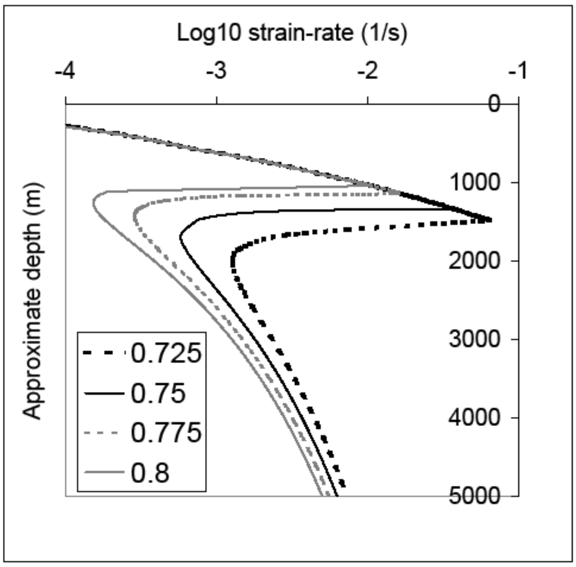
Log10 strain-rate (1/s)
-4
-3
-2
-1
0
1000
2000
3000
4000
5000
Approximate depth (m)
0.725
0.75
0.775
0.8

Figure 3:

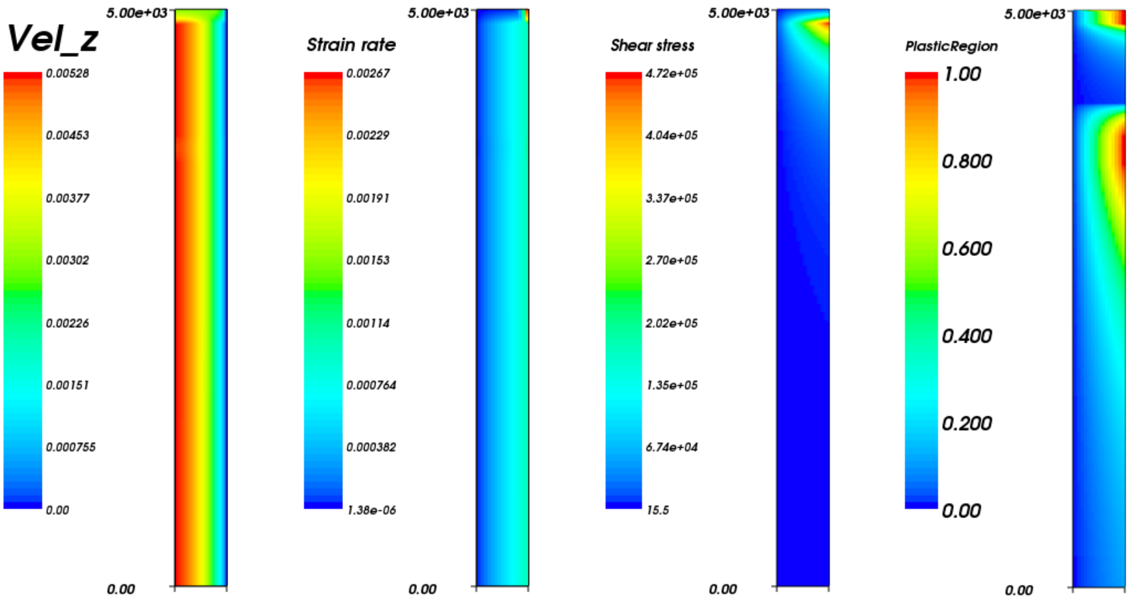
Vel_z
0.00528
0.00453
0.00377
0.00302
0.00226
0.00151
0.000755
0.00
5.00e+03
0.00
Strain rate
0.00267
0.00229
0.00191
0.00153
0.00114
0.000764
0.000382
1.38e-06
5.00e+03
0.00
Shear stress
4.72e+05
4.04e+05
3.37e+05
2.70e+05
2.02e+05
1.35e+05
6.74e+04
15.5
5.00e+03
0.00
PlasticRegion
1.00
0.800
0.600
0.400
0.200
0.00
5.00e+03
0.00

Forthcoming in Physics of The Earth and Planetary Interiors, DOI :10.1016/j.pepi.2007.05.001

Figure 4:

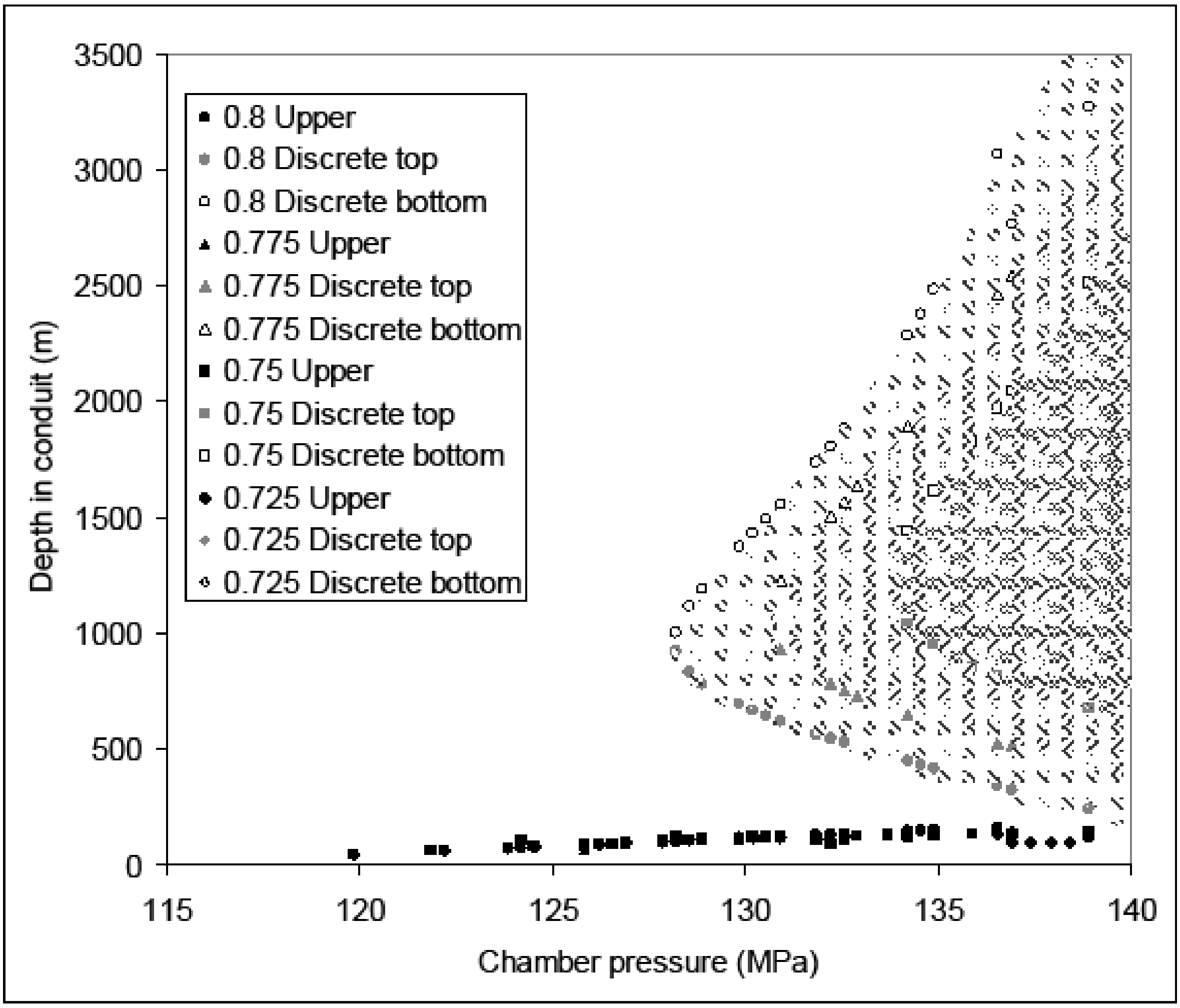

Figure 5:

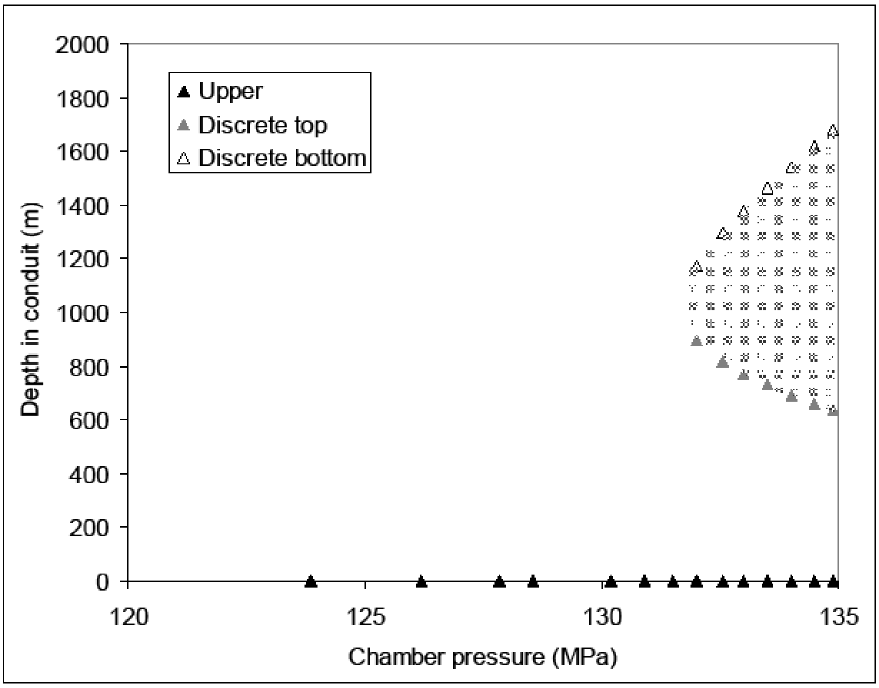

Upper
Discrete top
Discrete bottom
2000
1800
1600
1400
1200
1000
800
600
400
200
0
Depth in conduit (m)
120
125
130
135
Chamber pressure (MPa)

Figure 6:

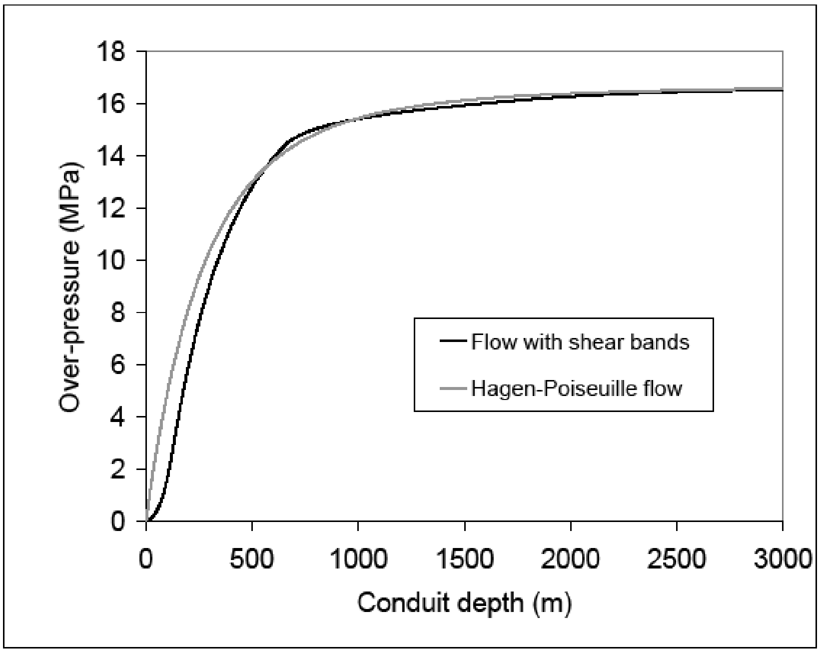
Over-pressure (MPa)
Conduit depth (m)
Flow with shear bands
Hagen-Poiseuille flow

Figure 7a:

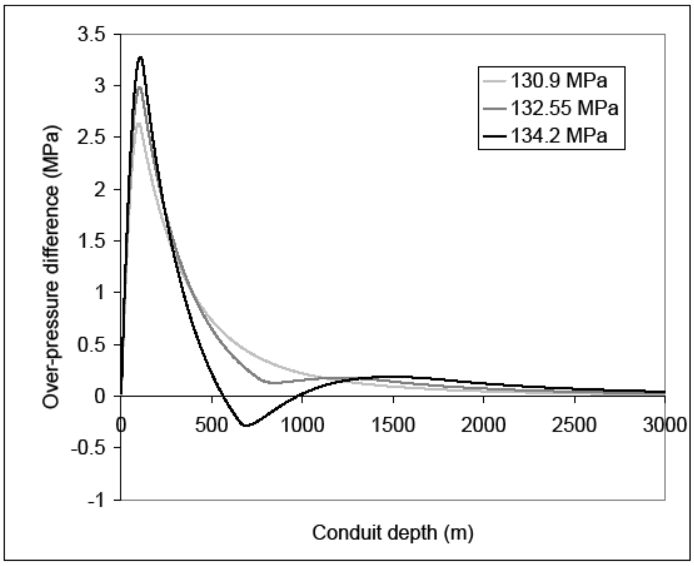
Over-pressure difference (MPa)
Conduit depth (m)
130.9 MPa
132.55 MPa
134.2 MPa

Figure 7b:

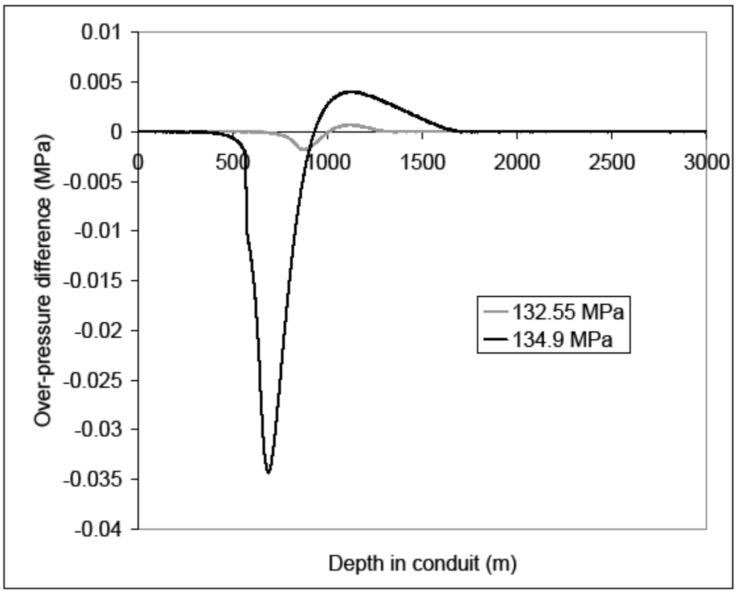
0.01
0.005
0
-0.005
-0.01
-0.015
-0.02
-0.025
-0.03
-0.035
-0.04
0
500
1000
1500
2000
2500
3000
Over-pressure difference (MPa)
Depth in conduit (m)
132.55 MPa
134.9 MPa